Journal of Controlled Release 355 (2023) 515–527

Contents lists available at ScienceDirect

Journal of Controlled Release

journal homepage: www.elsevier.com/locate/jconrel

Comparison of HER2-targeted affibody conjugates loaded with auristatin- and maytansine-derived drugs

Wen Yin [a,1], Tianqi Xu [b,1], Haozhong Ding [a], Jie Zhang [a], Vitalina Bodenko [c], Maria S. Tretyakova [c], Mikhail V. Belousov [d,e], Yongsheng Liu [b], Maryam Oroujeni [b], Anna Orlova [c,f,g], Vladimir Tolmachev [b,c], Torbjörn Gräslund [a,*], Anzhelika Vorobyeva [b,*]

[a] Department of Protein Science, KTH Royal Institute of Technology, Roslagstullsbacken 21, 114 17 Stockholm, Sweden
[b] Department of Immunology, Genetics and Pathology, Uppsala University, 751 85 Uppsala, Sweden
[c] Research Centrum for Oncotheranostics, Research School of Chemistry and Applied Biomedical Sciences, Tomsk Polytechnic University, 634050 Tomsk, Russia
[d] Siberian State Medical University, Ministry of Health of the Russian Federation, 634050 Tomsk, Russia
[e] National Research Tomsk Polytechnic University, 634050 Tomsk, Russia
[f] Department of Medicinal Chemistry, Uppsala University, 751 23 Uppsala, Sweden
[g] Science for Life Laboratory, Uppsala University, 751 23 Uppsala, Sweden

ARTICLE INFO

Keywords:
Affibody molecule
Drug conjugate
DM1
HER2
cancer
Therapy

ABSTRACT

Treatment with antibody drug conjugates targeting receptors over-expressed on cancer cells is well established for clinical use in several types of cancer, however, resistance often occurs motivating the development of novel drugs. We have recently investigated a drug conjugate consisting of an affibody molecule targeting the human epidermal growth factor receptor 2 (HER2), fused to an albumin-binding domain (ABD) for half-life extension, loaded with the cytotoxic maytansine derivative DM1. In this study, we investigated the impact of the cytotoxic payload on binding properties, cytotoxicity and biodistribution by comparing DM1 with the auristatins MMAE and MMAF, as part of the drug conjugate. All constructs had specific and high affinity binding to HER2, human and mouse albumins with values in the low- to sub-nM range. Z_{HER2}-ABD-mcMMAF demonstrated the most potent cytotoxic effect on several HER2-over-expressing cell lines. In an experimental therapy study, the MMAF-based conjugate provided complete tumor regression in 50% of BALB/c nu/nu mice bearing HER2-over-expressing SKOV3 tumors at a 2.9 mg/kg dose, while the same dose of Z_{HER2}-ABD-mcDM1 provided only a moderate anti-tumor effect. A comparison with the non-targeting Z_{Taq}-ABD-mcMMAF control demonstrated HER2-targeting specificity. In conclusion, a combination of potent cytotoxicity in vitro, with minimal uptake in normal organs in vivo, and efficient delivery to tumors provided a superior anti-tumor effect of Z_{HER2}-ABD-mcMMAF, while maintaining a favorable toxicity profile with no observed adverse effects.

1. Introduction

Targeted drug conjugates consist of affinity proteins coupled to highly potent cytotoxic drugs. The most common format is the antibody drug conjugate (ADC) [1], which is generated by conjugation of a monoclonal antibody (mAb) with a cytotoxic drug. Several ADCs have reached approval for clinical use by the US Food and Drug Administration (FDA), mostly as a second or third line therapy for patients with disseminated cancers, and many more are in clinical development. When developing targeted drug conjugates, a careful selection of the molecular target and optimization of the targeting protein is of great importance, as well as the choice of linker and drug.

Two commonly used classes of cytotoxic payloads are the maytansinoids and the auristatins, which both inhibit tubulin polymerization. Maytansine is a natural product, which can be found in the African shrub, *Maytenus ovatus* [2]. Maytansine was originally investigated in

* Corresponding authors.
E-mail addresses: wenyin@kth.se (W. Yin), tianqi.xu@igp.uu.se (T. Xu), haozhong@kth.se (H. Ding), jiezha@kth.se (J. Zhang), yongsheng.liu@igp.uu.se (Y. Liu), maryam.oroujeni@igp.uu.se (M. Oroujeni), anna.orlova@ilk.uu.se (A. Orlova), vladimir.tolmachev@igp.uu.se (V. Tolmachev), torbjorn@kth.se (T. Gräslund), anzhelika.vorobyeva@igp.uu.se (A. Vorobyeva).
[1] These authors contributed equally to this work

https://doi.org/10.1016/j.jconrel.2023.02.005
Received 2 September 2022; Received in revised form 8 December 2022; Accepted 1 February 2023
Available online 14 February 2023

clinical trials as a non-targeted chemotherapeutic cancer drug, but the results were disappointing with only few responders [3]. It was not until it was discovered that maytansine derivatives could be conjugated to mAbs for targeted therapy, that they found use as cytotoxic agents, since the systemic toxicity could then be managed [4]. The maytansine derivative DM1 (Fig. 1A) was later developed [5] and was conjugated to the mAb trastuzumab, which targets the human epidermal growth factor receptor 2 (HER2). The resulting conjugate, trastuzumab emtansine, was approved for clinical use by the FDA in 2013 for treatment of disseminated breast cancer [6]. Auristatin is derived from the natural product dolastatin 10 [7]. It has been derivatized and included in several ADCs approved for therapy or under clinical development [8]. Monomethyl auristatin E (MMAE, Fig. 1B) is a dolastatin 10 derivative that has found use as payload. It has, for example, been conjugated to an anti-CD30 antibody to create brentuximab vedotin, which is FDA approved for treatment of Hodgkin lymphoma (HL) and systemic anaplastic large cell lymphoma (ALCL) [9]. A more recent dolastatin 10 derivative is Monomethyl auristatin F (MMAF, Fig. 1C), which differs from MMAE by having one additional methyl group [10]. MMAF has also been conjugated to mAbs, and belantamab mafodotin is an anti-CD38-directed, MMAF-conjugated ADC, that was approved as first line treatment for multiple myeloma patients in 2020 [11]. Treament with belantamab mafodotin is often accompanied with ocular adverse events, which has been attributed to the MMAF drug. Patients receiving belantamab mafodotin therefore need careful monitoring of any ocular symptoms which might require treatment adjustment [12,13].

A number of different linkers has been used to connect the payload to the protein carrier. For belantamab mafodotin, a non-cleavable maleimidocaproyl (mc) linker was used, and for trastuzumab emtansine another type of non-cleavable thioether-containing MCC-linker was used. Cells targeted by conjugates with non-cleavable linkers internalize the construct, which is then transported to the lysosomes where the protein carrier is degraded, and the drug is released. Conversely, MMAE is usually connected to its protein carrier via a cleavable linker that releases the payload through different mechanisms after cell entry. In brentuximab vedotin, MMAE is connected to the mAb by a maleimidocaproyl-Val-Cit-PABC linker that can be cleaved by intracellular proteases, such as Cathepsin B, between the Val and Cit amino acids.

Recently, non-immunoglobulin (non-Ig) carriers of cytotoxic drugs have started to emerge [14,15]. While no such drugs have yet been approved for clinical use, their performance in pre-clinical and early clinical trials are sometimes impressive [14,16,17]. Affibody molecules are a class of small and robust, non-Ig, engineered scaffold affinity proteins (ESPs), consisting of 58 amino acids in an antiparallel three-helix fold. The affibody framework does not contain any cysteine amino acids, and numerous studies have utilized this property, by adding one (or more) cysteines into the ESP for site-specific attachment of different components using thiol-directed conjugation chemistry. Affibody molecules have been selected against a large number of target proteins [18], including cancer-relevant receptors, such as the insulin-like growth factor 1 receptor (IGF1R) [19], the human epidermal growth factor receptors 2 and 3 (HER2 and HER3) [20,21]. HER2 is an oncogenic receptor that is overexpressed in 20–30% of all breast cancers [22], and to a lesser extent in other types of cancers, such as e.g. gastric or ovarian carcinoma. The affibody molecule $Z_{HER2:2891}$ has previously been selected to interact with the HER2 receptor with strong affinity (equilibrium dissociation constant, K_D) of 65 pM [23]. Its first applications were centered on radionuclide molecular imaging [24]. Chelators have been conjugated to uniquely inserted cysteines in the affibody, followed by labeling with radionuclides for both positron emission tomography (PET) and single photon emission computed tomography (SPECT) imaging [25]. Radiolabeled affibody molecules for molecular imaging are in clinical development, and have shown an impressive targeting ability and imaging contrast of HER2-expressing tumors and metastases [26,27].

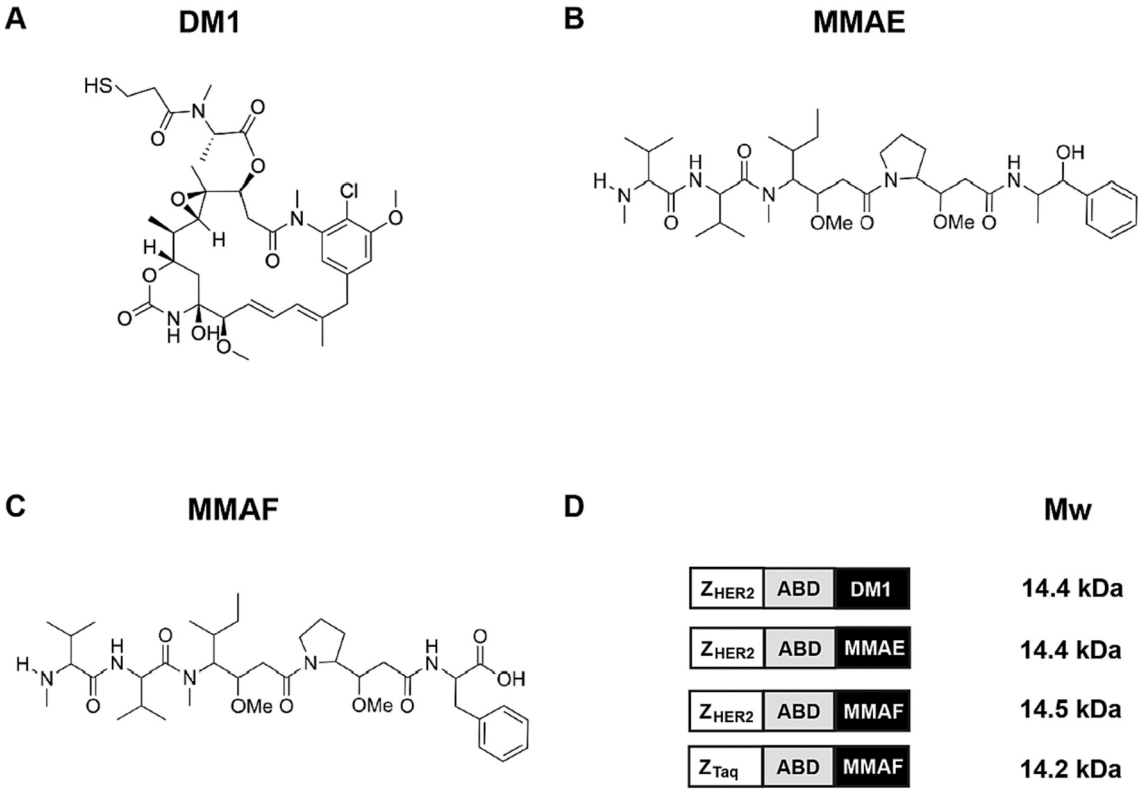

Fig. 1. Schematic representation of the cytotoxic drugs and conjugates. (A-C) The chemical structures of DM1, MMAE, and MMAF. (D) Schematic description of the drug conjugates with their molecular weights.

Affibody molecules are smaller than the molecular weight cut-off of the glomerular filter in the kidneys and are thus quickly eliminated from circulation. This is a desired trait when they are used for molecular imaging of tumors, since excellent contrast is obtained within hours after injection. However, for therapy applications, a longer half-life in circulation might be advantageous, as it increases the bioavailability of the compound. Utilization of affibody molecules as fusions to an albumin-binding domain (ABD) have previously been shown to increase the in vivo half-life dramatically [28]. In particular, the version ABD_{035} has sub-picomolar affinity to human serum albumin (HSA) [29], and has been found to extend the in vivo half-life of affibody-containing fusion proteins [28]. Upon injection, the ABD-containing protein quickly associates with the abundantly available serum albumin, which increases the size of the complex by 66.5 kDa, rendering it larger than the cut-off of the glomerular filter.

Affibody molecules have previously been conjugated to the maytansine derivative DM1 and investigated in a mouse model of HER2-positive ovarian cancer. The first conjugate included two affibody molecules and an ABD expressed as a head-to-tail hetero-trimer, $Z_{HER2:2891}$-$Z_{HER2:2891}$-ABD_{035}, with a cysteine in the C-terminus, where one DM1 molecule was attached via a mc-linker [15]. A potential issue with this construct was an elevated uptake in the liver. Such uptake might result in hepatic toxicity, which has often been found to be the limiting factor for the maximum tolerated dose, and should therefore be minimized [30]. The experimental therapy using $Z_{HER2:2891}$-$Z_{HER2:2891}$-ABD_{035}-mcDM1 was effective. However, after analysis of the study results it was hypothesized that the construct could be optimized to lower the uptake in the liver. New versions of the drug conjugate were generated, where three glutamic acids were inserted next to the cysteine, where DM1 was attached [31]. This modification led to 30% reduced uptake in the liver. A second generation drug conjugate has also been investigated, $Z_{HER2:2891}$-ABD_{035}-mcDM1, that contained only a single affibody molecule [16]. This variant was found to perform even better in a pre-clinical therapy study in mice bearing HER2-expressing xenografts and is currently the best performing affibody-drug conjugate targeting HER2 [16]. Another version with increased drug load from one to three was also evaluated [32]. While the amount of DM1 delivered to the tumors was increased by 1.5-fold, the conjugate was also taken up at a much higher rate in the liver, and was considered inferior to the version containing only one drug per affibody carrier.

In this study, we have investigated the impact of the cytotoxic payload on target binding, cytotoxicity and biodistribution of an ABD-fused affibody-drug conjugate. Since the affibody-ABD fusion protein does not contain any cysteine residue, a cysteine can be placed in the C-terminus to allow site-specific attachment of drugs. The best performing variant thus far, $Z_{HER2:2891}$-ABD_{035}-mcDM1 having three glutamic acids next to a single cysteine in the C-terminal end and conjugated to the maytansine derivative DM1, was used as a starting point (Fig. 1D). Two analogous conjugates were generated, where DM1 was replaced with the auristatin derivatives, MMAE or MMAF. We chose to use the same mc-linker to be able to compare the differences imposed by the drug, even though it has been found to be suboptimal for MMAE-loaded ADCs [10]. A non-targeting control construct, Z_{Taq}-ABD-mcMMAF, was also generated, which does not bind to any protein of mammalian origin. A tag with the amino acid sequence His-Glu-His-Glu-His-Glu was placed in the N-terminus of all conjugates. This tag has been shown to allow labeling with technetium-99m for investigation of the biodistribution [33–35]. The drug conjugates were extensively characterized and compared in vitro and in vivo. Subsequently, the $Z_{HER2:2891}$-ABD_{035}-mcMMAF conjugate was selected due to a more favorable biodistribution and was compared with $Z_{HER2:2891}$-ABD_{035}-mcDM1 for therapeutic efficiency in mice bearing HER2-overexpressing SKOV3 xenografts.

2. Materials and methods

2.1. General

All chemicals were from Thermo Fisher Scientific (Waltham, MA, USA), Merck (Darmstadt, Germany) or GE Healthcare (Uppsala, Sweden) unless stated otherwise.

2.2. Production of affibody-drug conjugates

The affibody used in this study was $Z_{HER2:2891}$ [23], herein labeled Z_{HER2}. The albumin binding domain (ABD) used for plasma half-life extension was ABD_{035} [29], herein labeled ABD. The affibody and the ABD were expressed as a fusion protein, Z_{HER2}-ABD [16], connected by a linker with the amino acid sequence Gly-Gly-Gly-Gly-Ser. A tag with the amino acid sequence Met-His-Glu-His-Glu-His-Glu for technetium-99m labeling was flanking the fusion protein in the N-terminus. The amino acids Glu-Glu-Glu-Cys were flanking the fusion protein in the C-terminus, where the cysteine was used for site-specific drug attachment.

The gene encoding a non-HER2 targeting control fusion protein, Z_{Taq}-ABD, was created by PCR amplification of the gene from a plasmid used in a previous study [15]. Z_{Taq} does not bind to any protein of human origin but to DNA polymerase from *Thermus aquaticus* [36]. During the amplification process, it was formatted similarly to Z_{HER2}-ABD, with sequences encoding an N-terminal Met-His-Glu-His-Glu-His-Glu extension, and a C-terminal Glu-Glu-Glu-Cys extension. In addition, sequences recognized by the NdeI and BamHI restriction enzymes were placed before and after the gene, respectively. The PCR product was purified by the Qiagen PCR purification kit (Qiagen, Hilden, Germany) according to the manufacturer's protocol, and was subcloned into the plasmid pET45b(+) (Novagen, Madison, WI, USA) using NdeI and BamHI restriction enzymes (New England Biolabs, Ipswitch, MA, USA). The Z_{Taq} and ABD genes were connected by a sequence encoding a linker with the same amino acids as Z_{HER2}-ABD, Gly-Gly-Gly-Gly-Ser. The expression cassette was validated by DNA sequencing (Eurofins Genomics, Ebersberg, Germany).

Both fusion proteins were produced in *Escherichia coli* and were purified by affinity chromatography with human serum albumin as immobilized ligand, as previously described [16]. After purification, Z_{HER2}-ABD and Z_{Taq}-ABD were lyophilized and stored at −80 °C for subsequent drug conjugation.

The lyophilized fusion proteins were dissolved in phosphate-buffered saline (PBS) (pH 6.6) to a concentration of 2 mg/mL. Then, freshly prepared tris (2-carboxyethyl) phosphine (TCEP) (0.5 M, dissolved in PBS buffer, pH 6.6) was added to the protein solution to a final concentration of 5 mM, followed by incubation for 1 h at 37 °C, to reduce potentially oxidized cysteines.

Three drugs, DM1, MMAE, and MMAF, with maleimidocaproyl (mc) linkers, were included in the study (Levena Biopharma, San Diego, CA, USA). The drugs were used freshly dissolved in DMSO at a concentration of 20 mg/mL. Each drug was added to the solution containing Z_{HER2}-ABD at a molar ratio of 3:1, followed by incubation at room temperature for 1 h. The resulting drug conjugates were labeled Z_{HER2}-ABD-mcDM1, Z_{HER2}-ABD-mcMMAE, and Z_{HER2}-ABD-mcMMAF. The non-HER2 targeting control Z_{Taq}-ABD-mcMMAF was produced in the same way. The reaction mixtures were subsequently purified by reversed-phase high-performance liquid chromatography (RP-HPLC). For the procedure, a Zorbax C18 SB column was used (Agilent, Santa Clara, CA, USA). Two buffers were included in the purification process, buffer A: water, and buffer B: acetonitrile. Both buffers were supplemented with 0.1% trifluoroacetic acid. The solutions containing the drug conjugates were loaded onto the column at 0% buffer B, and the column was washed with 30% buffer B, followed by elution with a linear gradient from 30% to 60% of buffer B during 30 min. The relevant fractions were pooled, lyophilized, and stored at −80 °C.

2.3. Characterization of affibody-drug conjugates

The affibody-drug conjugates were reconstituted in PBS and were subjected to biochemical characterization by sodium dodecyl sulphate-polyacrylamide gel electrophoresis (SDS-PAGE), analytical size-exclusion chromatography (SEC), analytical RP-HPLC, and liquid chromatography coupled electrospray ionization quadrupole time-of-flight mass spectrometry (ESI-qTOF). For SDS-PAGE, 10 μg of each construct was mixed with SDS-loading buffer, boiled for 10 min, and subsequently loaded on a NuPAGE bis-tris protein gel. Electrophoretic separation was carried out at 200 V for 1 h at 4 °C. The gel was stained with GelCode blue safe protein stain for 1 h, and destained in water. For analytical SEC, 5 μg of each conjugate was loaded on a pre-packed Superdex-75 5/150 column (GE Healthcare), equilibrated and subsequently eluted with PBS. The flow rate was 0.45 mL/min.

2.4. Affinity determination by a Biacore biosensor

Surface plasmon resonance analysis was employed for the determination of the kinetic constants of the interactions between the drug conjugates and HER2, HSA and mouse serum albumin (MSA). A Biacore T200 instrument (GE Healthcare) was used for the analysis. The extracellular domain of HER2 (Sino biological, Beijing, China) was immobilized on a CM5 chip (Cytiva, Uppsala, Sweden) using an amine coupling kit (Cytiva) at pH 4.65, according to the supplied protocol. Similarly, HSA (Novozymes, Bagsvaerd, Denmark) and MSA (Sigma-Aldrich, St. Louis, MO, USA), were immobilized on a second CM5 chip. On both chips, a blank surface was prepared by activation and deactivation via the amine coupling kit. The kinetic parameters were determined by single-cycle kinetic analysis with a flow rate of 50 μL/min at room temperature. The dilution series of the drug conjugates were 16, 32, 64, 128 and 256 nM. PBST (PBS with 0.005% Tween 20) was used as the running buffer, and 10 mM of glycine-HCl, pH 2.0, was used as the regeneration buffer.

2.5. Cell culture

The cell lines (SKOV3, SKBR3, AU565, BT474, A549 and MCF-7) were from the American Type Culture Collection (ATCC, purchased from LGC Promochem, Borås, Sweden). The SKOV3, SKBR3, AU565, BT474 cells were cultured in Roswell Park Memorial Institute (RPMI)-1640 medium (Biowest); the A549 and MCF7 cells were cultured in Dulbecco's Modified Eagle Medium (DMEM, Biowest). Both media were supplemented with 10% FBS (20% for BT474 cells) (Sigma-Aldrich), 2 mM L-glutamine and penicillin-streptomycin solution (Biowest). The cells were grown at 37 °C in 5% CO_2 atmosphere, unless stated otherwise.

2.6. Labeling with ^{99m}Tc

Labeling of the affibody-drug conjugates with technetium-99m at the N-terminal His-Glu-His-Glu-His-Glu peptide sequence was done according to a previously published protocol [16]. First, technetium-99m pertechnetate [^{99m}Tc]TcO_4^- was eluted from a ^{99}Mo/^{99m}Tc generator (Mallinckrodt, Petten, The Netherlands). To convert it to the [^{99m}Tc$(CO)_3(H_2O)_3]^+$ precursor, 500 μL (2.0–4.9 GBq) of [^{99m}Tc]TcO_4^- was added to a CRS kit vial (PSI, Villigen, Switzerland), followed by incubation at 100 °C for 30 min. After incubation, [^{99m}Tc$(CO)_3(H_2O)_3]^+$ was neutralized with an equal volume of HCl (0.1 M). Labeling was carried out by mixing the solution of [^{99m}Tc$(CO)_3(H_2O)_3]^+$ (19–60 μL, 80–180 MBq), with 40–80 μg (2.3–5.2 nmol, 33–75 μL in PBS) of each affibody-drug conjugate, followed by incubation at 60 °C for 60 min. After labeling, a 1000-fold molar excess of histidine (2.3–5.2 μmol) was added, with subsequent incubation at 60 °C for 10 min, to remove loosely-bound [^{99m}Tc$(CO)_3(H_2O)_3]^+$. The radiolabeled drug conjugates were purified using NAP-5 columns (GE Healthcare). The running buffer was PBS.

The stability of the radiolabel was evaluated by incubating the drug conjugates with a 1000-fold molar excess of histidine, dissolved in PBS, for up to 4 h. As a control experiment, the drug conjugates were incubated in PBS only.

The radiochemical yield and purity were investigated by instant thin-layer chromatography (iTLC) with PBS elution. The analysis of the iTLC strips were carried out using the CR35 BIO Plus Storage Phosphor System (ElysiaRaytest, Bietigheim-Bissingen, Germany). Images were analyzed by AIDA image analysis software (ElysiaRaytest).

2.7. Binding specificity and cellular processing

Specific binding of the ^{99m}Tc-labeled drug conjugates to cells was investigated according to a method described earlier [37]. Briefly, SKOV3, BT474, and SKBR3 cells were seeded in 6-well plates (10^6 cells/well) and were allowed to attach for 24 h. Non-radiolabeled drug conjugates (1000 nM) were added to one set of wells to saturate the HER2 receptors on the cells, while an equal volume of culture medium was added to another set of wells. The cells were incubated at room temperature for 30 min. Then, solutions containing the ^{99m}Tc-labeled drug conjugates were added to both sets of wells (2 nM final concentration), and incubated at 37 °C for 60 min. The medium was collected, and the cells were washed with PBS. Then, the cells were lysed by incubation with 1 M NaOH at 37 °C for 30 min, and cell debris were collected using a cell scraper. The activity in the media and in the cell lysates was measured by a gamma spectrometer equipped with a 3-in. NaI (TI) well detector (2480 Wizard, Wallac, Finland). The experiment was performed in triplicates.

The rate of binding of ^{99m}Tc-labeled drug conjugates to the cells and their internalization was investigated using a previously published protocol [37]. SKOV3 and BT474 cells were plated in 35 mm dishes (8×10^5 cells/dish) and were allowed to attach overnight. The next day, the media was removed and a drug conjugate (2 nM) in complete medium was added to the dishes, followed by incubation at 37 °C in 5% CO_2. Samples were collected at 1, 2, 4, 6 and 24 h for analysis. First, the medium was collected and the cells were washed with ice-cold PBS. To collect the membrane-bound activity, the cells were incubated with a 0.2 M glycine buffer containing 4 M urea (pH 2.0) for 5 min on ice. The solution was collected, the cells were washed with the same buffer, and combined, with the total activity considered as the membrane-bound fraction. Thereafter, the cells were lysed with 1 M NaOH for 30 min at 37 °C and the solution was collected. Cell debris were detached from the dish with a scraper, the dishes were washed with PBS, and the solutions were combined, with the total activity considered as the internalized fraction. The activity in the medium, the membrane-bound fractions and the internalized fractions was measured using an automatic gamma spectrometer as described above.

2.8. Measurement of affinity to living cells

A LigandTracer Yellow instrument (Ridgeview Instruments, Vänge, Sweden) was used to measure the affinity of the drug conjugates to HER2-expressing SKOV3 cells, according to a previously described method [16]. For each measurement, 2×10^6 cells were seeded to a local area of an 89-mm cell culture dish, and were allowed to attach for 24 h. Increasing concentrations (1, 2 and 5 nM) of radiolabeled drug conjugates were added to each dish followed by measurement of cell-associated activity. Then, the medium containing drug conjugate was replaced with medium only, and the dissociation phase was recorded overnight. The measurements were performed at room temperature. The obtained data were corrected for radionuclide decay, followed by analysis by the TraceDrawer software (Ridgeview Instruments), to determine the equilibrium dissociation constants (K_D values) of the interactions. The data were subjected to an Interaction Map analysis (Ridgeview Diagnostics, Uppsala, Sweden) to estimate the heterogeneity

of the interactions.

2.9. In vitro cytotoxicity measurement of the affibody-drug conjugates

Approximately 5000 cells/well (2000 cells/well for SKOV3) were seeded in a 96-well plate and were allowed to attach for 24 h. Series of concentrations of the drug conjugates were added to the wells, followed by incubation in a humidified incubator for 72 h. The cell viability was measured using the Cell Counting Kit 8 (CCK-8; Sigma, St. Louis, MO, USA) according to the protocol supplied by the manufacturer.

2.10. Animal studies

The animal experiments were carried out in agreement with the Swedish legislation on animal welfare and were approved by the Animal Research Committee at Uppsala University (permit 5.8.18–11931/2020, approved 28 August 2020).

2.11. Biodistribution in tumor-bearing mice

To study the biodistribution, 36 female BALB/c nu/nu mice were implanted with 10^7 SKOV3 cells in 100 μL of medium subcutaneously (s.c.) on the hind leg. The biodistribution experiment was performed 3 weeks after the implantation. The mice were randomized into 9 groups ($n = 4$). The average weight of the animals was 19.3 ± 1.1 g. Each animal received an intravenous (i.v.) injection of 6 μg of a radiolabeled drug conjugate. The administered activity was 60 kBq for 4 h, 640 kBq for 24 h, and 10.2 MBq for 48 h time points. At each time–point, the mice were weighed and anesthetized by an intraperitoneal (i.p.) injection of a ketamine-xylazine solution (30 μL of solution per gram body weight; ketamine 10 mg/mL; xylazine 1 mg/mL), followed by heart puncture. The animals were dissected, and the blood, organs, and tissues were isolated and weighted, followed by measurement of activity using an automatic gamma spectrometer, as described previously. The uptake was calculated as the percentage of injected dose per gram of sample (% ID/g).

2.12. Experimental therapy

For the experimental therapy study, thirty-seven female BALB/c nu/nu mice were implanted with 10^7 SKOV3 cells in 100 μL of medium subcutaneously (s.c.) on the abdomen. The mice were randomized to four groups (n = 8–10) one week after the implantation. The mice received intravenous injections of 2.9 mg/kg of Z_{HER2}-ABD-mcMMAF, Z_{HER2}-ABD-mcDM1, Z_{Taq}-ABD-mcMMAF or PBS. The injections were performed once per week for five consecutive weeks at day 0, day 7, day 14, day 21, and day 28.

The body weights and tumor volumes were monitored at least twice per week. The average body weight was 17.7 ± 1.0 g at day 0 when the treatment started (17.7 ± 1.4 g, 17.8 ± 0.6 g, 17.6 ± 1.0 g, 17.7 ± 1.1 g in the Z_{HER2}-ABD-mcMMAF, Z_{HER2}-ABD-mcDM1, Z_{Taq}-ABD-mcMMAF and PBS groups, respectively, with no significant difference between the groups, $p > 0.05$). The tumors were measured for the largest longitudinal (length) and transverse (width) diameter with a digital caliper and the volumes were calculated using the formula: tumor volume = 1/2 (length × width^2). The average tumor volume was 85 ± 19 mm^3 and the group tumor volume was 80 ± 21 mm^3, 83 ± 17 mm^3, 93 ± 14 mm^3, 84 ± 25 mm^3 in the Z_{HER2}-ABD-mcMMAF, Z_{HER2}-ABD-mcDM1, Z_{Taq}-ABD-mcMMAF and PBS groups, respectively, at day 0 (no significant difference between the groups, $p > 0.05$). The mice were euthanized at a predetermined humane end-point when the tumor volume reached 1 cm^3, tumor ulceration occurred on the tumor surface, 10% weight loss in less than a week or a total of 15% weight loss. The study duration was 90 days according to the requirements of the ethical permit. After the mice were sacrificed, kidneys and livers were collected, placed in 10% formalin for 24 h and stored in 70% ethanol at 4 °C. The tissue samples of two mice from the Z_{HER2}-ABD-mcMMAF, Z_{HER2}-ABD-mcDM1 and PBS groups (groups A, B and D, respectively) were used for pathological examination performed by a veterinary pathologist at BioVet AB veterinary diagnostic laboratory (Sollentuna, Sweden).

2.13. Statistical analysis

For determination of statistically significant differences, a two-tailed unpaired t-test was used when comparing two values, and a one-way ANOVA with Bonferroni post-hoc correction was used when comparing multiple values. The signs: * correspond to $p < 0.05$, ** to $p < 0.01$, *** to $p < 0.001$, **** to $p < 0.0001$. The survival data were analyzed using Mantel-Cox log-rank test. The therapy outcomes (no response, partial response, sustained remission, complete remission) were analyzed by a chi-square test. The analyses were carried out using Prism, version 9.3.1 (Graphpad Software, San Diego, CA, USA).

3. Results

3.1. Production and initial characterization of affibody-drug conjugates

To compare the functionality of affibody conjugates loaded with different cytotoxic drugs, new auristatin-containing drug conjugates were generated and their characteristics were compared to Z_{HER2}-ABD-mcDM1 [14] (Fig. 1D). First, the two fusion proteins Z_{HER2}-ABD and Z_{Taq}-ABD were expressed in *Escherichia coli* and were purified by column chromatography. After recovery in a pure form, DM1, MMAE, and MMAF were conjugated to the unique C-terminal cysteine introduced to both fusion proteins, followed by further purification with reversed-phase high-performance liquid chromatography (RP-HPLC). Samples of the material recovered from the RP-HPLC purification were analyzed by SDS-PAGE (Fig. 2A).

The drug conjugates were of high purity and of essentially the correct molecular weight. The drug conjugates were further analyzed under native conditions by size-exclusion chromatography (Fig. 2B). They were eluted as relatively symmetrical peaks, although, with some tailing. From Fig. 2B it can be concluded that the drug conjugates were in a mono-disperse form, and that there were no obvious degradation products. All four constructs were analyzed by analytical RP-HPLC (Fig. 2C) and were eluted as single peaks. Integration of the area under curve showed that they were of high purity (above 95%). The Z_{HER2}-ABD-mcMMAE and Z_{HER2}-ABD-mcMMAF conjugates were eluted slightly later than the Z_{HER2}-ABD-DM1, indicating more hydrophobic constructs. The non-targeting control construct Z_{Taq}-ABD-mcMMAF was eluted last, indicating the most hydrophobic construct. Further, the molecular weights of the drug conjugates were determined by mass spectrometry. The results matched the theoretical molecular weights with a difference of <2 Da in all cases (Fig. S1, Table S1).

3.2. Interaction of the affibody-drug conjugates with HER2, HSA and MSA

Further characterization of the drug conjugates ensued, where the affinities to their intended targets, HER2 and serum albumins, were determined using a Biacore biosensor (Fig. S2, Table 1). The three HER2-targeting drug conjugates showed strong affinity of similar strength to HER2 with equilibrium dissociation constants (K_D values) ranging from 0.33 nM to 0.46 nM. The affinities of the HER2-targeting drug conjugates to HSA were also strong and ranged from 0.088 to 0.24 nM. The affinities of the HER2-targeting drug conjugates to mouse serum albumin (MSA) were weaker than the affinities to HSA in all cases. From the sensorgrams in Fig. S2, it is evident that the dissociation phase is faster, compared with the sensorgrams recorded for the interactions with HSA. For the interactions with MSA, there is a surprising four- to five-fold stronger affinity of Z_{HER2}-ABD-mcDM1 (0.28 ± 0.01 nM), compared to Z_{HER2}-ABD-mcMMAE (1.2 ± 0.1 nM), and Z_{HER2}-ABD-mcMMAF (1.4 ±

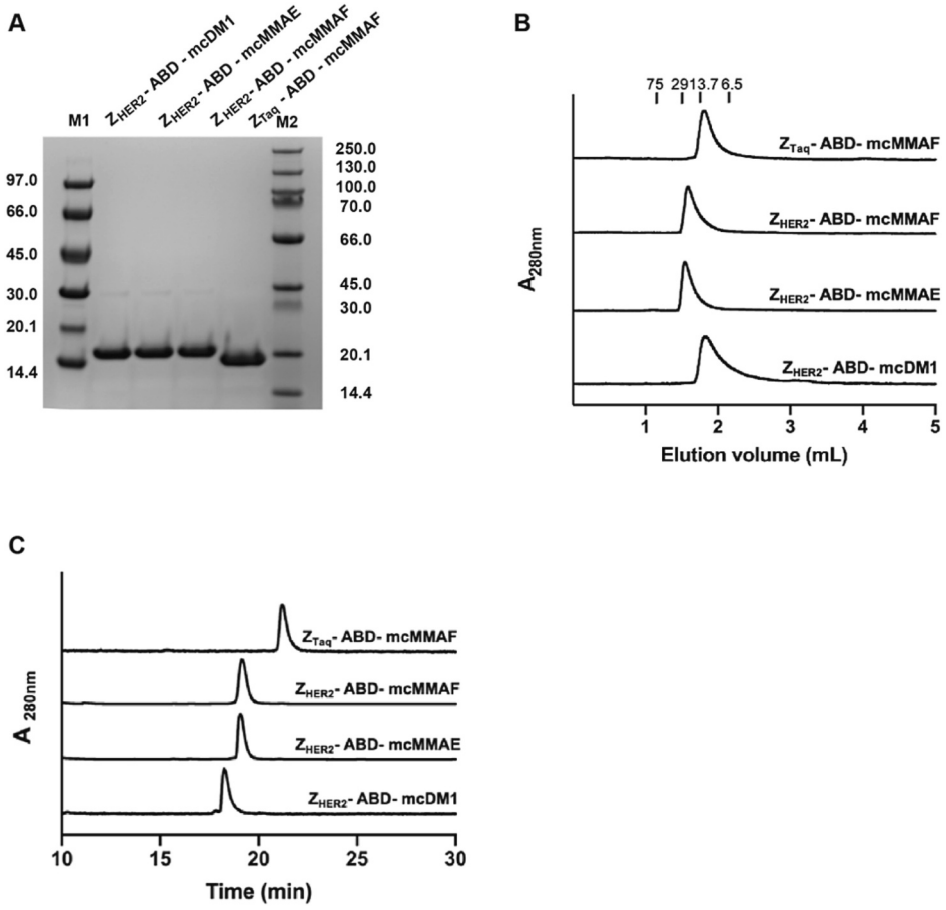

Fig. 2. Characterization of the affibody-drug conjugates investigated in this study. (A) SDS-PAGE gel of the drug conjugates after purification. 10 μg of the final product is loaded in each lane. The samples in lanes M1 and M2 are marker proteins with their molecular weights indicated to the left and right of the gel, respectively. (B) Analysis of the drug conjugates (5 μg each) by size-exclusion chromatography. (C) RP-HPLC analysis of the drug conjugates.

Table 1
Equilibrium dissociation constants (K_D) for interactions between the drug conjugates and HER2, HSA and MSA. Each value is the average of three independent measurements ±1 standard deviation (SD).

Drug conjugate	HER2 (nM)	HSA (nM)	MSA (nM)
Z_{HER2}-ABD-mcMMAE	0.38 ± 0.01	0.088 ± 0.01	1.2 ± 0.1
Z_{HER2}-ABD-mcMMAF	0.46 ± 0.01	0.24 ± 0.14	1.4 ± 0.1
Z_{HER2}-ABD-mcDM1	0.33 ± 0.01	0.091 ± 0.005	0.28 ± 0.01
Z_{Taq}-ABD-mcMMAF	NB*	1.92 ± 0.02	5.85 ± 0.05

* NB = No binding was detected.

0.1 nM). The non-targeting control, Z_{Taq}-ABD-mcMMAF, had an unexpectedly weaker affinity to both MSA and HSA than the three HER2-targeting drug conjugates, due to a slightly slower on-rate and a slightly faster off-rate.

3.3. Radiolabeling, cell binding and cellular processing of the affibody-drug conjugates

To further analyze the binding properties of the drug conjugates, the specificity of their interaction with HER2 overexpressing cells and their rate of internalization were measured. For these experiments, the drug conjugates were site-specifically labeled with [^{99m}Tc]Tc(CO)$_3$ using the N-terminal chelating peptide His-Glu-His-Glu-His-Glu.

The results of the radiolabeling reactions showed a high radiochemical yield of 94–96% for all conjugates (n = 6–8) (Table S2). After purification, a radiochemical purity over 97% was obtained for all conjugates. To test the stability of the radiolabel, the labeled drug conjugates were incubated with a 1000-fold molar excess of histidine in PBS or PBS (control) for 4 h. The results showed no release of the label for the MMAE and MMAF conjugates, and a minor label release of 2–3% for the DM1 conjugate in both the histidine and the control samples, showing robust radiolabeling of the drug conjugates.

The interaction of the ^{99m}Tc-labeled drug conjugates with the HER2 overexpressing cell lines SKBR3, SKOV3, and BT474, was studied by incubating the cells with the ^{99m}Tc-labeled drug conjugates in the presence or absence of the same drug conjugate lacking the radiolabel (Fig. S3A). When the receptors were pre-blocked with a large excess of non-labeled drug conjugate, a significant decrease in cell-bound radioactivity was observed for all three drug conjugates in all three cell lines, showing that the binding interaction was specific and HER2-mediated.

To study internalization, the radiolabeled drug conjugates were incubated with the SKOV3 and BT474 cell lines and the rates of association and internalization were measured over 24 h (Fig. 3). The three drug conjugates quickly associated with SKOV3 cells reaching a plateau by 4–6 h post-addition, and were efficiently internalized. The internalized fractions for [^{99m}Tc]Tc-labeled Z_{HER2}-ABD-mcMMAE, Z_{HER2}-ABD-mcMMAF, and Z_{HER2}-ABD-mcDM1 were 37 ± 2%, 36 ± 2%, 40 ± 0%, respectively, at 24 h in SKOV3 cells. The internalized fraction was lower in BT474 compared to SKOV3 at 24 h: 27 ± 2%, 27 ± 3%, 31 ± 2% for [^{99m}Tc]Tc-labeled Z_{HER2}-ABD-mcMMAE, Z_{HER2}-ABD-mcMMAF, and Z_{HER2}-ABD-mcDM1, respectively.

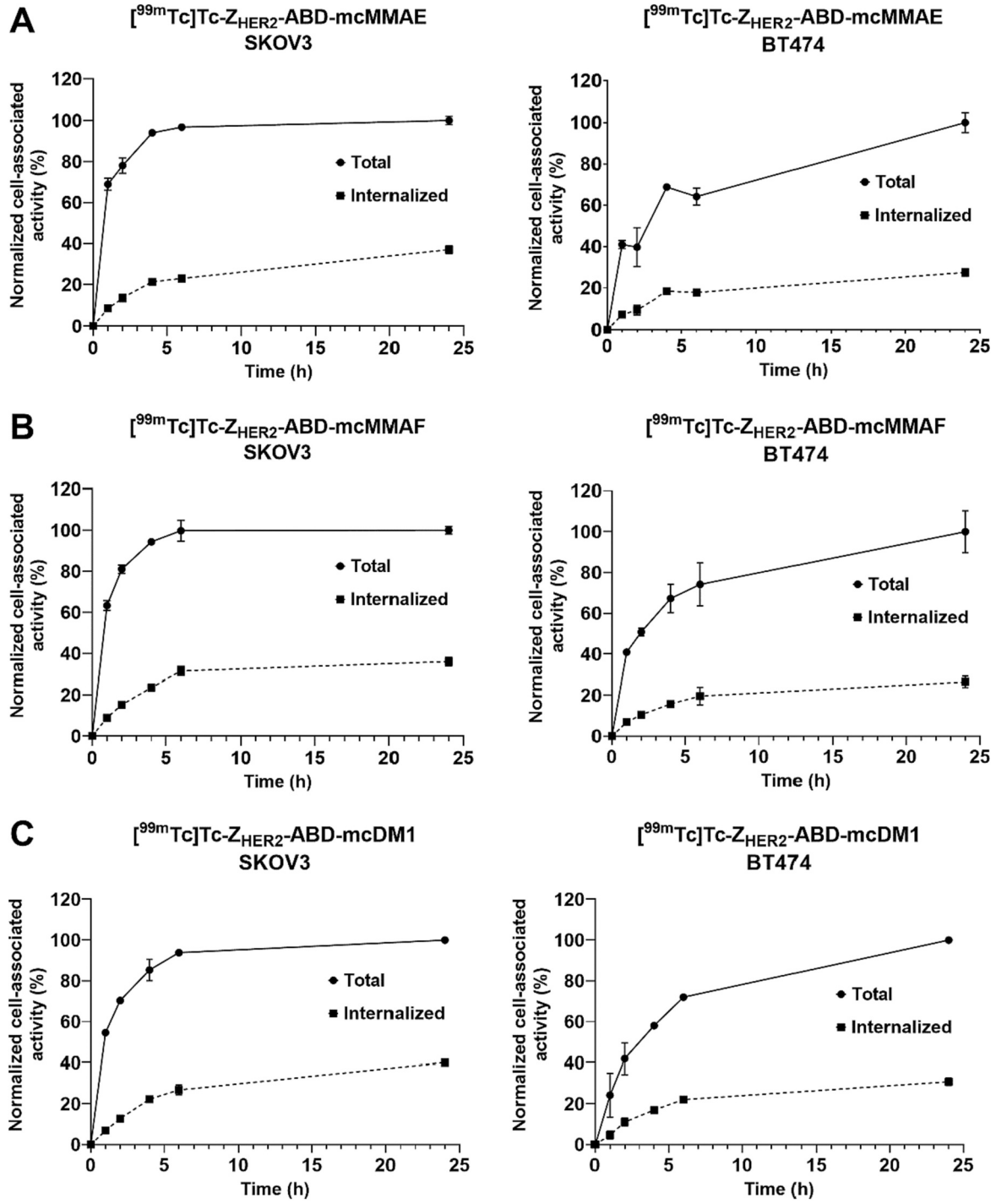

Fig. 3. Determination of the rates of association and internalization of the radiolabeled drug conjugates in SKOV3 (left panels) and BT474 (right panels) cells. The cells were incubated with [^{99m}Tc]Tc-labeled (A) Z_{HER2}-ABD-mcMMAE, (B) Z_{HER2}-ABD-mcMMAF, and (C) Z_{HER2}-ABD-mcDM1 over 24 h and the rate of association and internalization is plotted as a function of time. Each data point is an average of three independent experiments, and the error bars correspond to 1 SD.

3.4. Real-time binding analysis of the affibody-drug conjugates and the SKOV3 cells

The binding of [^{99m}Tc]Tc-labeled Z_{HER2}-ABD-mcMMAE, Z_{HER2}-ABD-mcMMAF, and Z_{HER2}-ABD-mcDM1 to living SKOV3 cells was measured using a LigandTracer Yellow instrument (Table 2). Rapid binding and slow dissociation was observed for all three labeled compounds (Fig. S3B). The InteractionMaps derived from the real-time binding analysis (Fig. S3C) showed one major interaction with a stronger affinity and one minor interaction with a weaker affinity. The equilibrium dissociation constants (K_D) for the major interactions were not significantly different ($p > 0.05$) and were 0.44 ± 0.03 nM, 0.41 ± 0.02 nM, and 0.56 ± 0.20 nM for [^{99m}Tc]Tc-labeled Z_{HER2}-ABD-mcMMAE, Z_{HER2}-ABD-mcMMAF, and Z_{HER2}-ABD-mcDM1, respectively.

3.5. Cytotoxicity of the affibody-drug conjugates

In order to compare the potencies of the affibody-drug conjugates containing auristatins or the maytansine, HER2-expressing cell lines were incubated with concentration series of the drug conjugates, and the

Table 2
Equilibrium dissociation constants for the high affinity (K_{D1}) and the low affinity (K_{D2}) interactions between ^{99m}Tc-labeled affibody-drug conjugates and HER2-overexpressing SKOV3 cells.

Drug conjugate	K_{D1} (nM)	Weight (%)	K_{D2} (nM)	Weight (%)
[^{99m}Tc]Tc-Z_{HER2}-ABD-mcDM1	0.44 ± 0.03	58 ± 1	13.6 ± 0.6	25 ± 1
[^{99m}Tc]Tc-Z_{HER2}-ABD-mcMMAE	0.41 ± 0.02	54 ± 1	15.5 ± 5.9	29 ± 0
[^{99m}Tc]Tc-Z_{HER2}-ABD-mcMMAF	0.56 ± 0.20	58 ± 4	18.4 ± 2.9	26 ± 1

viability of the cells was measured (Table 3, Fig. S4). Four cell lines with high HER2 expression were included, the ovarian cancer cell line SKOV3 and the breast cancer cell lines SKBR3, AU565 and BT474, as well as lung adenocarcinoma cell line A549 with moderate/low HER2 expression.

Among the cell lines with high HER2 expression, the BT474 cell line was the most resistant to the cytotoxic action of the drug conjugates. The BT474 cell line was only affected by Z_{HER2}-ABD-mcMMAF with an IC_{50} value of 0.01 nM and with a survival of 40% to 50% of the cells. It was not affected by Z_{HER2}-ABD-mcMMAE or Z_{HER2}-ABD-mcDM1. In SKOV3 cells, a remarkable difference in IC_{50} values was observed among the three drug conjugates. While Z_{HER2}-ABD-mcMMAF was the most potent (IC_{50} value of 12 nM), Z_{HER2}-ABD-mcDM1 showed a 40-fold lower potency. Conversely, Z_{HER2}-ABD-mcMMAE did not affect the viability of SKOV3 cells at any of the concentrations. It was even so that at the highest concentration included (1000 nM), an effect of the non-targeted control Z_{Taq}-ABD-mcMMAF was observed, but none for Z_{HER2}-ABD-mcMMAE. The SKBR3 and AU565 cell lines were more sensitive to the cytotoxic action of all conjugates compared to SKOV3. For SKBR3 cells, the Z_{HER2}-ABD-mcDM1 and Z_{HER2}-ABD-mcMMAE drug conjugates were 10-fold less potent than Z_{HER2}-ABD-mcMMAF. For AU565 cells, Z_{HER2}-ABD-mcMMAF was also found to be the most potent, with a 10-fold lower IC_{50} value compared to Z_{HER2}-ABD-mcDM1, and a 100-fold lower IC_{50} value compared to Z_{HER2}-ABD-mcMMAE. The moderate/low-HER2 expressing cell line A549 was affected to a much smaller extent by the drug conjugates than the high-HER2 expressing cell lines. Moreover, there was only a minor effect of Z_{HER2}-ABD-mcMMAE and Z_{HER2}-ABD-mcMMAF on the low-HER2 expressing cell line, MCF-7 (Fig. S4). The non-targeting control Z_{Taq}-ABD-mcMMAF was 10 to 1000 times less potent compared to Z_{HER2}-ABD-mcMMAF to the high-HER2 expressing cell lines, had a minor effect on A549 cells, and showed no effect on MCF-7 cells. Clearly, Z_{HER2}-ABD-mcMMAF was the most potent drug conjugate in this experiment.

3.6. Biodistribution of the affibody-drug conjugates in mice bearing SKOV3 xenografts

To analyze the tumor targeting ability and compare the uptake of the affibody-drug conjugates in normal organs and tissues, female BALB/c nu/nu mice, bearing SKOV3 xenografts, were intravenously injected with the radiolabeled drug conjugates and the uptake of radioactivity in the tumor and in the organs was quantified at 4, 24 and 48 h post-injection (Table S3).

The differences in uptake between the three drug conjugates were more pronounced at 4 h post-injection, than at later time points. At 4 h the blood retention was significantly higher for [^{99m}Tc]Tc-Z_{HER2}-ABD-mcMMAE (16 ± 2 %ID/g), than for [^{99m}Tc]Tc-Z_{HER2}-ABD-mcDM1 (12 ± 0 %ID/g) and [^{99m}Tc]Tc-Z_{HER2}-ABD-mcMMAF (7 ± 1 %ID/g) (Fig. 4A). A small, however, significant ($p < 0.05$) difference between the blood retention of [^{99m}Tc]Tc-Z_{HER2}-ABD-mcMMAF and [^{99m}Tc]Tc-Z_{HER2}-ABD-mcDM1 was also observed at 24 and 48 h. The activity in the majority of normal organs was decreasing over time. By contrast, the uptake in the tumor was increasing over time, except for [^{99m}Tc]Tc-Z_{HER2}-ABD-mcMMAE with a tendency to decrease from 24 to 48 h. For all conjugates the liver uptake was relatively low (below 10 %ID/g) and the kidney uptake was predominant, ranging from 80 to 90 %ID/g, indicating renal clearance.

The comparison of tumor uptake of the affibody-drug conjugates showed that [^{99m}Tc]Tc-Z_{HER2}-ABD-mcMMAF and [^{99m}Tc]Tc-Z_{HER2}-ABD-mcDM1 had similar tumor uptake at all time points (Fig. 4C). [^{99m}Tc]Tc-Z_{HER2}-ABD-mcMMAE had a significantly ($p < 0.05$) higher tumor uptake at 4 h and a tendency to higher tumor accumulation in comparison to the other two conjugates. The comparison of liver uptake showed that [^{99m}Tc]Tc-Z_{HER2}-ABD-mcMMAF had a significantly ($p < 0.05$) lower uptake in liver at 4 h and an overall lower liver accumulation than the other conjugates (Fig. 4B). The activity in the liver was plotted as a function of time and the area under the curve (AUC) was calculated (Fig. 4B). The AUC values were similar for the Z_{HER2}-ABD-mcMMAE and Z_{HER2}-ABD-mcDM1 conjugates, while ZHER2-ABD-mcMMAF had a 1.14-fold lower AUC value than the DM1-containing conjugate. The combination of low blood, liver and spleen uptake together with high tumor accumulation of [^{99m}Tc]Tc-Z_{HER2}-ABD-mcMMAF and the potent cytotoxicity in vitro, made it a promising candidate for evaluation in experimental therapy study.

3.7. Experimental therapy

The anti-tumor effect of Z_{HER2}-ABD-mcMMAF was studied in female BALB/c nu/nu mice bearing SKOV3 xenografts and was compared with Z_{HER2}-ABD-mcDM1, which demonstrated an impressive anti-tumor effect in one of our previous studies [16]. The control groups included mice receiving Z_{Taq}-ABD-mcMMAF (non-targeting control) and mice receiving PBS (vehicle control). Based on the potent cytotoxic effect of Z_{HER2}-ABD-mcMMAF in vitro, the administered dose of 2.9 mg/kg was chosen to be lower than the doses of Z_{HER2}-ABD-mcDM1 used in our previous studies (10.3 and 15.1 mg/kg [16]) in order to prevent the potential off-target toxicities of the MMAF-conjugate and to determine whether Z_{HER2}-ABD-mcMMAF would provide a more potent anti-tumor effect than Z_{HER2}-ABD-mcDM1 when used at equal doses.

The tumor growth of individual mice is presented in Fig. S5 and Table S4. The average tumor volumes at the beginning of the therapy were 80 ± 21 mm^3 (Z_{HER2}-ABD-mcMMAF), 83 ± 17 mm^3 (Z_{HER2}-ABD-mcDM1), 93 ± 14 mm^3 (Z_{Taq}-ABD-mcMMAF) and 84 ± 25 mm^3 (PBS). There was no significant difference ($p > 0.05$) between the tumors volumes in the different groups at the treatment start (day 0) (Fig. S6A). Already at day 7, mice receiving Z_{HER2}-ABD-mcMMAF had significantly ($p < 0.01$) smaller tumors than mice receiving Z_{Taq}-ABD-mcMMAF (Fig. S6B). At day 35, after four treatment cycles, mice receiving Z_{HER2}-ABD-MMAF had significantly ($p < 0.001$) smaller tumors than the mice in both control groups. The tumors in the control groups grew rapidly (Fig. S5). The tumor growth in the Z_{HER2}-ABD-mcMMAF group (tumor doubling time 31 d, 95% CI from 21 to 49 d) and the Z_{HER2}-ABD-mcDM1 group (tumor doubling time 19 d, 95% CI from 14 to 25 d) was inhibited compared to tumor growth in the Z_{Taq}-ABD-mcMMAF group (tumor doubling time 10 d, 95% CI from 8 to 12 d) and the PBS group (tumor doubling time 12 d, 95% CI from 9 to 16 d).

Table 3
The cytotoxicity of the drug conjugates to HER2-expressing cell lines.

Cell line	IC_{50} (nM)			
	Z_{HER2}-ABD-mcDM1	Z_{HER2}-ABD-mcMMAE	Z_{HER2}-ABD-mcMMAF	Z_{Taq}-ABD-mcMMAF
SKOV3	412	ND	12	190
SKBR3	1.4	8.2	0.2	170
AU565	2.5	24	0.2	180
BT474	ND	ND	0.01	110
A549	ND	ND	215	ND

ND = Not determined.

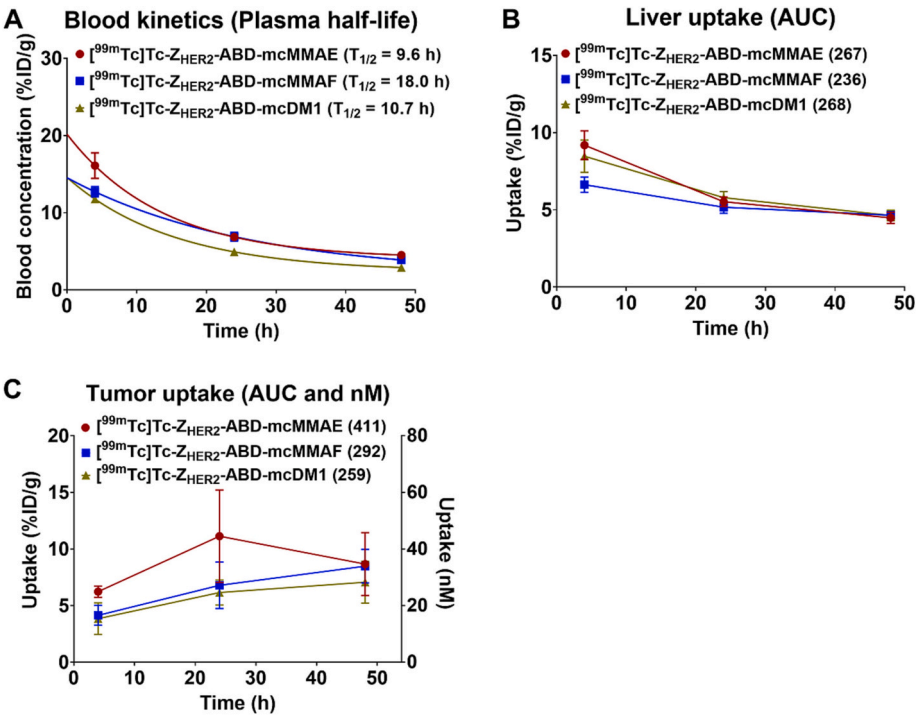

Fig. 4. Comparison of (A) blood concentration, (B) tumor uptake, and (C) liver uptake of the radiolabeled affibody-drug conjugates at 4, 24 and 48 h. AUC refers to the area under curve and is given in parenthesis after the names of the constructs in panels B and C Each data point is the average of the measured radioactivity in four animals and the error bars correspond to 1 SD.

The survival curves and therapeutic outcomes are shown in Fig. 5. In both the Z_{Taq}-ABD-mcMMAF and the PBS control groups, all mice had exponential tumor growth and were euthanized between days 35 and 57. By the end of the study the median survival was not reached for Z_{HER2}-ABD-mcMMAF group, while it was 56 days for the Z_{HER2}-ABD-mcDM1 group, 42 days for the Z_{Taq}-ABD-mcMMAF group, and 46 days for PBS group. This resulted in a significantly ($p < 0.01$) longer median survival in the Z_{HER2}-ABD-mcMMAF group than in all other groups and significantly ($p < 0.05$) longer median survival in the Z_{HER2}-ABD-mcDM1 group compared to both control groups (Fig. 5A).

In the Z_{HER2}-ABD-mcMMAF group, five out of ten (50%) mice had complete remission without any visible tumor at the study termination (90 d), two out of ten (20%) mice had sustained remission with macroscopic tumors at the study termination, while three out of ten (30%) mice had partial response with delayed tumor growth (10%) or tumor ulceration without tumor growth (20%). In the Z_{HER2}-ABD-mcDM1 group, two out of ten (20%) mice had complete remission, three out of ten (30%) of mice had a partial response, while five out of ten (50%) mice did not respond to the treatment (Fig. 5B).

No significant ($p > 0.05$) difference was observed in animal weight between the groups during the duration of the study, indicating that the treatments were well tolerated (Fig. 5C). A pathology examination did not find any macroscopical lesions in the liver or the kidneys. A mild increase in microvesicular fatty change in mouse A8, a slight karyocytomegaly in mice A8 and B5, and hepatocellular mitotic figures in mouse D6 were observed (Fig. S7). All of these changes were considered to be within the normal variation for the animal groups. Mice A10, B7, B9 and D8 had a minimal score of glomerulopathy and were considered to be background lesions (Fig. S8).

4. Discussion

Targeted drug conjugates have become one of the most important additions for efficient cancer therapy over the last 10 to 20 years. Several antibody-drug conjugates (ADCs) are now approved by regulatory authorities for clinical use [8,38]. Furthermore, drug conjugates based on alternative scaffolds also show promising results in preclinical evaluation [14,16,17], and may become important additions to cancer therapies in the future. Alternative scaffolds are generally smaller than the mAbs used in ADCs and may therefore penetrate tumors better [39] for a more efficient therapeutic effect. Furthermore, alternative scaffold affinity proteins, such as affibody molecules, lack cysteine amino acids, which allows for incorporation of cysteine amino acids at desired positions, where the cytotoxic drugs can be attached. This allows for creation of homogenous compounds with control of the number and spatial distribution of the drugs, which is more difficult for ADCs, even though site-specific drug attachment strategies are under development [40]. A study comparing an ADC (brentuximab vedotin) with and without site-specific drug attachment, suggests that site-specific drug attachment leads to improved pharmacokinetics and is better tolerated [41].

A majority of the approved drugs have a warhead consisting of a cytotoxic tubulin polymerization inhibitor derived from maytansine or auristatin. These compounds were originally evaluated as chemotherapeutic drugs, but the development was abandoned. Since they are potent and the side effects are severe; only low doses were tolerated by the patients, resulting in few responders [3]. However, it is now evident that when the drugs are conjugated to a targeting moiety (e.g. a protein), the potency and side-effects can be controlled. To comprehensively study the properties of drug conjugates employing these molecules is a challenging task due to their extreme cytotoxic effect, as well as to the fact that antibody-drug conjugates usually consist of a heterogeneous mixture of species with different drug-to-antibody ratios and spatial arrangement of the drugs, both of which influences their properties.

Here, we have carefully evaluated drug conjugates consisting of an affibody molecule targeting HER2, coupled to an ABD for in vivo half-life extension, and one of the cytotoxic tubulin polymerization inhibitors, MMAE, MMAF, or DM1, connected using a maleimidocaproyl linker. The drugs were attached to a unique cysteine placed in the C-terminus of the fusion protein. This allowed spatial control of the

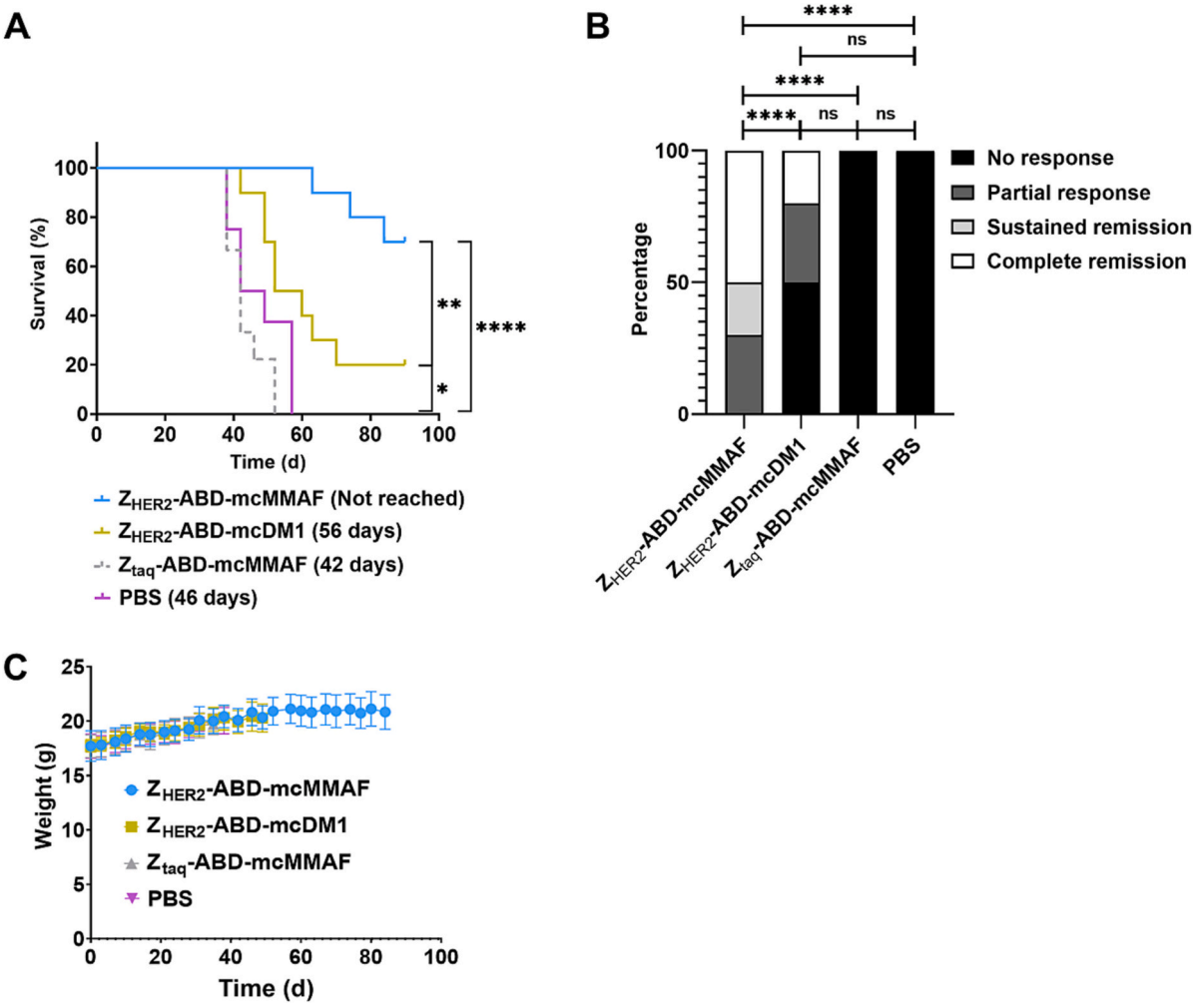

Fig. 5. In vivo experimental therapy. (A) Survival of BALB/c nu/nu mice bearing SKOV3 xenografts after five treatment cycles with 2.9 mg/kg of Z_{HER2}-ABD-mcMMAF, Z_{HER2}-ABD-mcDM1, Z_{Taq}-ABD-mcMMAF (non-targeting control) or PBS (vehicle only), and (B) therapy outcomes for the different treatment groups (n = 8–10). The outputs categories were defined as no response (exponentional tumor growth), partial response (delayed tumor growth or tumor ulceration without growth), sustained remission (macroscopic tumors at the study termination) and complete remission (no tumors at the study termination). The difference between the groups was determined using a chi-square test. The stars correspond to significant differences, where * corresponds to $p < 0.05$, ** corresponds to $p < 0.01$, and **** corresponds to $p < 0.0001$. (C) Average animal weight in each group during therapy. The data are presented as an average value of 8–10 mice ± SD. The curves are drawn until 30–33% of the mice in a group were euthanized.

conjugation reaction and facile production of homogenous conjugates with one drug per protein carrier.

Biochemical characterization of the drug conjugates showed that under native conditions all three drug conjugates are in a monodisperse state when analyzed by passage through a size-exclusion column, even though they contained relatively hydrophobic cytotoxic drugs, that might interact in an unspecific manner. This was an important property, since multimerization of drug conjugates may lead to an elevated clearance in vivo. In our earlier studies, Z_{HER2}-ABD-mcDM1 has also shown the same monodisperse nature [16]. When further analyzing the affinities of the individual domains toward their intended targets, some interesting observations were made. While the affinities to HER2 were similar among the conjugates, the affinities to HSA and MSA appeared to vary to some extent. Since the attached drug is closer to the ABD, which interacts with HSA and MSA, than to the affibody molecule interacting with HER2, some differences in the influence of the drugs on the protein carrier were observed. However, the affinities to the intended targets were in all cases stronger than what was believed to be the minimum needed for efficient targeting in vivo.

Further characterization of the cytotoxic potential showed some interesting differences between the drug conjugates. For the HER2 overexpressing cell lines SKOV3, SKBR3, BT474, and AU565, Z_{HER2}-ABD-mcMMAF was more potent than the other two conjugates. For the BT474 cell line, only Z_{HER2}-ABD-mcMMAF was able to affect the viability of the cells to any extent, and a relatively large portion of the cells (approximately 40%) appeared to be unaffected. A minor effect was seen for a subset of the cells when treated with Z_{HER2}-ABD-mcDM1. The resistance mechanism of the BT474 cell line to the tubulin polymerization inhibitors is presently not known, but the cell line was clearly more sensitive to MMAF than to DM1. When MMAE is used as a payload in an antibody drug conjugate, such as brentuximab vedotin, it is usually coupled by a cleavable maleimidocaproyl-Val-Cit-PABC linker [42]. In a study by Doronina et al., combinations of the MMAE or MMAF drugs linked to an anti-CD30 antibody were evaluated, which later lead to the development of brentuximab vedotin [10]. For the ADC, where MMAE was attached with the maleimidocaproyl-Val-Cit-PABC linker, the IC_{50} towards CD30-overexpressing cells was 0.18 nM, while it was considerably weaker (> 50 nM) when linked with the non-cleavable mc-linker, which is the same linker as is used in this study. When MMAF was attached to the same antibody, as investigated by Doronina et al., the IC_{50} values were 0.03 and 0.065 nM for the maleimidocaproyl-Val-Cit-PABC or the maleimidocaproyl linker, respectively. These data suggest

that MMAF is more potent than MMAE. They also point to a better suitability of the maleimidocaproyl-Val-Cit-PABC linker for linking MMAE to the protein carrier. In future studies, it would be interesting to investigate drug conjugates consisting of Z_{HER2}-ABD and MMAE, conjugated via the maleimidocaproyl-Val-Cit-PABC linker and compare the results obtained for Z_{HER2}-ABD-mcMMAE. The comparison of IC_{50} values obtained in different studies is challenging, since the affinity of the targeting protein to the receptor might differ, as well as the rate of receptor internalization when engaged by the drug conjugate, both of which are important parameters for intracellular delivery of the cytotoxic drug. Furthermore, different cell lines could be affected to different degrees by drug conjugates, which was also found in this study, where for example the IC_{50} of Z_{HER2}-ABD-mcMMAF ranged from 0.01 to 12 nM for the SKOV3, AU565, BT474, and SKBR3 cell lines, which all have a high expression level of HER2. Previous studies on ADCs have shown that differences in the sensitivity between different cell lines can be attributed to differences in the expression level of multidrug resistance proteins, such as MDR1, impairment of receptor internalization, as well as impairment of the lysosomal transport and degradation machinery [43–45]. It is likely that the differences in sensitivity of the different cell lines to Z_{HER2}-ABD-mcMMAF can be attributed to a combination of these factors.

To allow investigation of cell binding, cellular processing, and biodistribution of the drug conjugates, they were radiolabeled with technetium-99m tricarbonyl. The labeling was site-specific and located on the N-terminal His-Glu-His-Glu-His-Glu tag, to minimize any interference of the label with the functionality of the domains or the drug. Cell binding and cellular processing were studied in two cell lines with high HER2 expression, SKOV3 and BT474. Some differences between the cell lines were observed, where the association and internalization were faster for SKOV3 cells compared to BT474 cells. This further corroborates that there are differences in the rate of receptor internalization between different cell lines. The rate of internalization by cancer cells is an important parameter that has a major impact on the ability of the drug conjugates to provide the cytotoxic effect. The intracellular fraction of the drug conjugates in SKOV3 cells was similar, and ranged from 37 to 40%. These values are in a good agreement with our earlier study on Z_{HER2}-ABD-mcDM1 [16]. The affinities to living SKOV3 cells were also determined for the drug conjugates and ranged from 0.41 to 0.46 nM, which agreed well with the values determined to the extracellular domain of the HER2 receptor using a Biacore instrument (0.33 to 0.46 nM). In addition to the major interaction, a weaker interaction between the drug conjugates and the cells was also found. Similar secondary interactions have earlier been observed between monomeric affibody molecules or ADAPTs and HER2 [46,47].

The comparison of the biodistribution of the radiolabeled affibody-drug conjugates showed that [^{99m}Tc]Tc-Z_{HER2}-ABD-mcMMAE had the highest tumor uptake, while the tumor uptake of [^{99m}Tc]Tc-Z_{HER2}-ABD-mcMMAF and [^{99m}Tc]Tc-Z_{HER2}-ABD-mcDM1 was similar. The uptake of the drug conjugates in normal organs followed a pattern similar to the earlier study with [^{99m}Tc]Tc-Z_{HER2}-ABD-mcDM1 [16]. The uptake in kidneys was relatively high and the uptake in liver was relatively low, suggesting predominant clearance by the kidneys. [^{99m}Tc]Tc-Z_{HER2}-ABD-mcMMAF had the lowest liver uptake among the three drug conjugates. Low uptake in the liver is beneficial as it has earlier been shown that minimizing the liver uptake may lead to a higher tolerated dose of a drug conjugate [41].

Z_{HER2}-ABD-mcDM1 has previously been shown efficacious for treatment of HER2-overexpressing tumors in a pre-clinical mouse model [16]. In the current study, Z_{HER2}-ABD-mcMMAF demonstrated potent anti-tumor effect in SKOV3 xenografts with efficient tumor growth inhibition and significantly prolonged survival with a complete remission rate of 50%. This effect was apparently due to the targeted delivery of MMAF since the non-targeted control compound Z_{Taq}-ABD-mcMMAF did not show any anti-tumor effect and the tumors in this group grew exponentially. The mice receiving Z_{HER2}-ABD-mcDM1 also had significantly prolonged survival compared to the mice in the control groups, with a complete remission rate of 20%, however, half of the mice did not respond to the treatment at the dose used in the current study. The dose of Z_{HER2}-ABD-mcMMAF and Z_{HER2}-ABD-mcDM1 was 0.2 mol/kg (2.9 mg/kg) in the current study, the same dose as used for the dimeric Z_{HER2}-Z_{HER2}-ABD-mcDM1 conjugate in Altai et al. [15], where Z_{HER2}-Z_{HER2}-ABD-mcDM1 demonstrated therapeutic efficiency in SKOV3 xenografts. The dose of 0.2 mol/kg is lower than the doses of Z_{HER2}-ABD-mcDM1 (0.72 mol/kg and 1.05 mol/kg) used by Xu et al. [16]. Since the tumor uptake of [^{99m}Tc]Tc-Z_{HER2}-ABD-mcDM1 and [^{99m}Tc]Tc-Z_{HER2}-ABD-mcMMAF was similar, while Z_{HER2}-ABD-mcMMAF appeared to be more cytotoxic than Z_{HER2}-ABD-mcDM1 in HER2-positive cells in vitro (Table 3, Fig. S4, Table S3), we hypothesized that a lower dose of Z_{HER2}-ABD-mcMMAF would provide more potent anti-tumor effect, while the same dose of Z_{HER2}-ABD-mcDM1 would be less effective. The results of experimental therapy confirmed our hypothesis, showing that Z_{HER2}-ABD-mcMMAF provided a more pronounced therapeutic effect than Z_{HER2}-ABD-mcDM1 at equal doses. Histopathological examination of livers and kidneys from mice that received Z_{HER2}-ABD-mcMMAF, Z_{HER2}-ABD-mcDM1, and vehicle control did not find any lesions that would suggest toxicity of the treatment regimens. The ADC trastuzumab emtansine (T-DM1) has earlier been investigated in a subcutaneous SKOV-3 model in mice [48]. When dosed at 30 mg/kg T-DM1 was able to completely eradicate the implanted tumors, and when dosed at 10 mg/kg, complete regression without regrowth was observed in three out of five mice. The dose used in the present study (0.2 mol/kg) approximately corresponds to a dose of 15 mg/kg in the study by Yu and co-workers. It appears that a the AffiDCs have to be administered slightly more frequently or at slightly higher doses compared to T-DM1.

In summary, the characteristics of three affibody-drug conjugates have been compared in this study. Z_{HER2}-ABD-mcMMAE demonstrated the lowest cytotoxicity in vitro and would probably benefit from a cleavable linker, such as the maleimidocaproyl-Val-Cit-PABC between the drug and the protein carrier. Both the Z_{HER2}-ABD-mcMMAF and Z_{HER2}-ABD-mcDM1 drug conjugates showed a suitable biodistribution profile. A combination of a potent cytotoxic effect in vitro with high tumor uptake in vivo provided a superior anti-tumor effect of Z_{HER2}-ABD-mcMMAF at lower doses in comparison to the previously developed Z_{HER2}-ABD-mcDM1, while maintaining a favorable toxicity profile with low liver uptake. The Z_{HER2}-ABD-mcMMAF affibody-drug conjugate is a promising agent for HER2-targeted therapy of cancer.

CRediT authorship contribution statement

Wen Yin: Formal analysis, Investigation, Data curation, Writing – original draft, Writing – review & editing. **Tianqi Xu:** Formal analysis, Investigation, Data curation, Writing – original draft, Writing – review & editing, Visualization. **Haozhong Ding:** Formal analysis, Investigation, Data curation. **Jie Zhang:** Formal analysis, Investigation, Data curation, Writing – original draft, Writing – review & editing. **Vitalina Bodenko:** Formal analysis, Investigation, Data curation, Writing – review & editing. **Maria S. Tretyakova:** Formal analysis, Investigation, Data curation, Writing – review & editing. **Mikhail V. Belousov:** Investigation, Writing – review & editing, Supervision, Project administration. **Yongsheng Liu:** Investigation, Data curation, Writing – review & editing. **Maryam Oroujeni:** Investigation, Data curation, Writing – review & editing. **Anna Orlova:** Investigation, Resources, Writing – review & editing, Supervision, Project administration, Funding acquisition. **Vladimir Tolmachev:** Conceptualization, Formal analysis, Investigation, Resources, Data curation, Writing – review & editing, Supervision, Funding acquisition. **Torbjörn Gräslund:** Conceptualization, Formal analysis, Writing – original draft, Writing – review & editing, Visualization, Supervision, Project administration, Funding acquisition. **Anzhelika Vorobyeva:** Conceptualization, Validation, Formal analysis, Investigation, Data curation, Writing – original draft, Writing – review &

editing, Visualization, Supervision, Project administration, Funding acquisition.

Declaration of Competing Interest

Anna Orlova and Vladimir Tolmachev own shares in Affibody AB (Solna, Sweden). The other authors declare no conflict of interest.

Data availability

Data will be made available on request.

Acknowledgments

This research was funded by the Swedish Agency for Innovation, VINNOVA (2019/00104), VR 2019-00994 (V. T.) and the Swedish Cancer Society, Cancerfonden (CAN 21 1861 Pj (T.G.); 2020/181 (A.V.); 20 0893 Pj (A.V.); 20 0815 PjF (A.O.)).

Appendix A. Supplementary data

Supplementary data to this article can be found online at https://doi.org/10.1016/j.jconrel.2023.02.005.

References

[1] P. Khongorzul, C.J. Ling, F.U. Khan, A.U. Ihsan, J. Zhang, Antibody-drug conjugates: a comprehensive review, Mol. Cancer Res. 18 (2020) 3–19.
[2] B.R. Hearn, S.J. Shaw, D.C. Myles, Microtubule targeting agents, in: Comprehensive medicinal chemistry II, 2007, pp. 81–110.
[3] J.M. Cassady, K.K. Chan, H.G. Floss, E. Leistner, Recent developments in the maytansinoid antitumor agents, Chem. Pharm. Bull. 52 (2004) 1–26.
[4] R.V.J. Chari, B.A. Martell, J.L. Gross, S.B. Cook, S.A. Shah, W.A. Blättler, S. J. McKenzie, V.S. Goldmacher, Immunoconjugates containing novel maytansinoids: promising anticancer drugs, Cancer Res. 52 (1992) 127–131.
[5] G.D. Lewis Phillips, G. Li, D.L. Dugger, L.M. Crocker, K.L. Parsons, E. Mai, W. A. Blättler, J.M. Lambert, R.V.J. Chari, R.J. Lutz, et al., Targeting HER2-positive breast cancer with trastuzumab-DM1, an antibody-cytotoxic drug conjugate, Cancer Res. 68 (2008) 9280–9290.
[6] S. Verma, D. Miles, L. Gianni, I.E. Krop, M. Welslau, J. Baselga, M. Pegram, D.-Y. Oh, V. Diéras, E. Guardino, et al., Trastuzumab emtansine for HER2-positive advanced breast cancer, N. Engl. J. Med. 367 (2012) 1783–1791.
[7] G.R. Pettit, Y. Kamano, C.L. Herald, A.A. Tuinman, F.E. Boettner, H. Kizu, J. M. Schmidt, L. Baczynskyi, K.B. Tomer, R.J. Bontems, The isolation and structure of a remarkable marine animal antineoplastic constituent: Dolastatin 10, J. Am. Chem. Soc. 109 (1987) 6883–6885.
[8] Z. Fu, S. Li, S. Han, C. Shi, Y. Zhang, Antibody drug conjugate: the "biological missile" for targeted cancer therapy, Signal Transduct. Target. Ther. (2022) 7.
[9] A. Younes, N.L. Bartlett, J.P. Leonard, D.A. Kennedy, C.M. Lynch, E.L. Sievers, A. Forero-Torres, Brentuximab Vedotin (SGN-35) for relapsed CD30-positive lymphomas, N. Engl. J. Med. 363 (2010) 1812–1821.
[10] S.O. Doronina, B.A. Mendelsohn, T.D. Bovee, C.G. Cerveny, S.C. Alley, D.L. Meyer, E. Oflazoglu, B.E. Toki, R.J. Sanderson, R.F. Zabinski, et al., Enhanced activity of monomethylauristatin F through monoclonal antibody delivery: effects of linker technology on efficacy and toxicity, Bioconjug. Chem. 17 (2006) 114–124.
[11] S. Lonial, H.C. Lee, A. Badros, S. Trudel, A.K. Nooka, A. Chari, A.O. Abdallah, N. Callander, N. Lendvai, D. Sborov, et al., Belantamab mafodotin for relapsed or refractory multiple myeloma (DREAMM-2): a two-arm, randomised, open-label, phase 2 study, Lancet Oncol. 21 (2020) 207–221.
[12] A. Wahab, A. Rafae, K. Mushtaq, A. Masood, H. Ehsan, M. Khakwani, A. Khan, Ocular toxicity of belantamab mafodotin, an oncological perspective of management in relapsed and refractory multiple myeloma, Front. Oncol. 11 (2021) 1–6.
[13] S. Lonial, A.K. Nooka, P. Thulasi, A.Z. Badros, B.H. Jeng, N.S. Callander, H. A. Potter, D. Sborov, B.E. Zaugg, R. Popat, et al., Management of belantamab mafodotin-associated corneal events in patients with relapsed or refractory multiple myeloma (RRMM), Blood Cancer J. (2021) 11.
[14] F. Brandl, S. Busslinger, U. Zangemeister-Wittke, A. Plückthun, Optimizing the anti-tumor efficacy of protein-drug conjugates by engineering the molecular size and half-life, J. Control. Release 327 (2020) 186–197.
[15] M. Altai, H. Liu, H. Ding, B. Mitran, P.-H. Edqvist, V. Tolmachev, A. Orlova, T. Gräslund, Affibody-derived drug conjugates: potent cytotoxic molecules for treatment of HER2 over-expressing tumors, J. Control. Release 288 (2018) 84–95.
[16] T. Xu, H. Ding, A. Vorobyeva, M. Oroujeni, A. Orlova, V. Tolmachev, T. Gräslund, Drug conjugates based on a monovalent affibody targeting vector can efficiently eradicate HER2 positive human tumors in an experimental mouse model, Cancers (Basel). 13 (2021) 85.
[17] G. Bennett, A. Brown, G. Mudd, P. Huxley, K. Rietschoten, S. Pavan, L. Chen, S. Watcham, J. Lahdenranta, N. Keen, MMAE delivery using the bicycle toxin conjugate BT5528, Mol. Cancer Ther. 19 (2020) 1385–1394.
[18] S. Ståhl, T. Gräslund, A. Eriksson Karlström, F.Y. Frejd, P.Å. Nygren, J. Löfblom, Affibody molecules in biotechnological and medical applications, Trends Biotechnol. 35 (2017) 691–712.
[19] J. Li, E. Lundberg, E. Vernet, B. Larsson, I. Hoiden-Guthenberg, T. Graslund, Selection of affibody molecules to the ligand-binding site of the insulin-like growth factor-1 receptor, Biotechnol. Appl. Biochem. 55 (2010) 99–109.
[20] M. Wikman, A.C. Steffen, E. Gunneriusson, V. Tolmachev, G.P. Adams, J. Carlsson, S. Ståhl, Selection and characterization of HER2/neu-binding affibody ligands, Protein Eng. Des. Sel. 17 (2004) 455–462.
[21] M. Malm, N. Kronqvist, H. Lindberg, L. Gudmundsdotter, T. Bass, F.Y. Frejd, I. Höidén-Guthenberg, Z. Varasteh, A. Orlova, V. Tolmachev, et al., Inhibiting HER3-mediated tumor cell growth with Affibody molecules engineered to low Picomolar affinity by position-directed error-prone PCR-like diversification, PLoS One 8 (2013), e62791.
[22] D.J. Slamon, G.M. Clark, S.G. Wong, W.J. Levin, A. Ullrich, W.L. McGuire, Human breast cancer: correlation of relapse and survival with amplification of the HER-2/neu oncogene, Science 235 (1987) 177–182.
[23] J. Feldwisch, V. Tolmachev, C. Lendel, N. Herne, A. Sjöberg, B. Larsson, D. Rosik, E. Lindqvist, G. Fant, I. Höidén-Guthenberg, et al., Design of an optimized scaffold for affibody molecules, J. Mol. Biol. 398 (2010) 232–247.
[24] A. Orlova, M. Magnusson, T.L.J. Eriksson, M. Nilsson, B. Larsson, I. Höiden-Guthenberg, C. Widström, J. Carlsson, V. Tolmachev, S. Ståhl, et al., Tumor imaging using a picomolar affinity HER2 binding Affibody molecule, Cancer Res. 66 (2006) 4339–4348.
[25] V. Tolmachev, A. Orlova, J. Sörensen, The emerging role of radionuclide molecular imaging of HER2 expression in breast cancer, Semin. Cancer Biol. 72 (2021) 185–197.
[26] J. Sörensen, I. Velikyan, D. Sandberg, A. Wennborg, J. Feldwisch, V. Tolmachev, A. Orlova, M. Sandström, M. Lubberink, H. Olofsson, et al., Measuring HER2-receptor expression in metastatic breast cancer using [68Ga]ABY-025 Affibody PET/CT, Theranostics 6 (2016) 262–271.
[27] J. Sörensen, D. Sandberg, M. Sandström, A. Wennborg, J. Feldwisch, V. Tolmachev, G. Åström, M. Lubberink, U. Garske-Román, J. Carlsson, et al., First-in-human molecular imaging of HER2 expression in breast cancer metastases using the 111In-ABY-025 affibody molecule, J. Nucl. Med. 55 (2014) 730–735.
[28] V. Tolmachev, A. Orlova, R. Pehrson, J. Galli, B. Baastrup, K. Andersson, M. Sandström, D. Rosik, J. Carlsson, H. Lundqvist, et al., Radionuclide therapy of HER2-positive microxenografts using a 177Lu-labeled HER2-specific Affibody molecule, Cancer Res. 67 (2007) 2773–2782.
[29] A. Jonsson, J. Dogan, N. Herne, L. Abrahmsén, P.Å. Nygren, Engineering of a femtomolar affinity binding protein to human serum albumin, Protein Eng. Des. Sel. 21 (2008) 515–527.
[30] S. Babai, L. Auclert, H. Le-Louët, Safety data and withdrawal of hepatotoxic drugs, Therapies 76 (2021) 715–723.
[31] H. Ding, M. Altai, S.S. Rinne, A. Vorobyeva, V. Tolmachev, T. Gräslund, A. Orlova, Incorporation of a hydrophilic spacer reduces hepatic uptake of HER2-targeting Affibody–DM1 drug conjugates, Cancers (Basel). 11 (2019) 1168–1187.
[32] H. Ding, T. Xu, J. Zhang, V. Tolmachev, M. Oroujeni, A. Orlova, T. Gräslund, A. Vorobyeva, Affibody-derived drug conjugates targeting HER2: effect of drug load on cytotoxicity and biodistribution, Pharmaceutics 13 (2021) 430.
[33] C. Hofström, A. Orlova, M. Altai, F. Wangsell, T. Gräslund, V. Tolmachev, Use of a HEHEHE purification tag instead of a hexahistidine tag improves biodistribution of affibody molecules site-specifically labeled with 99mTc, 111In, and 125I, J. Med. Chem. 54 (2011) 3817–3826.
[34] C. Hofström, M. Altai, H. Honarvar, J. Strand, J. Malmberg, S.J. Hosseinimehr, A. Orlova, T. Gräslund, V. Tolmachev, HAHAHA, HEHEHE, HIHIHI, or HKHKHK: influence of position and composition of histidine containing tags on biodistribution of [99mTc(CO) 3]+−labeled affibody molecules, J. Med. Chem. 56 (2013) 4966–4974.
[35] V. Tolmachev, C. Hofström, J. Malmberg, S. Ahlgren, S.J. Hosseinimehr, M. Sandström, L. Abrahmsén, A. Orlova, T. Gräslund, HEHEHE-tagged affibody molecule may be purified by IMAC, is conveniently labeled with [99mTc(CO)3]+, and shows improved biodistribution with reduced hepatic radioactivity accumulation, Bioconjug. Chem. 21 (2010) 2013–2022.
[36] E. Gunneriusson, K. Nord, M. Uhlén, P. Nygren, Affinity maturation of a Taq DNA polymerase specific affibody by helix shuffling, Protein Eng. 12 (1999) 873–878.
[37] H. Wållberg, A. Orlova, Slow internalization of anti-HER2 synthetic affibody monomer 111In-DOTA-ZHER2:342-pep2: implications for development of labeled tracers, Cancer Biother. Radiopharm. 23 (2008) 435–442.
[38] C. Do Pazo, K. Nawaz, R.M. Webster, The oncology market for antibody-drug conjugates, Nat. Rev. Drug Discov. 20 (2021) 583–584.
[39] I. Nessler, E. Khera, S. Vance, A. Kopp, Q. Qiu, T.A. Keating, A.O. Abu-Yousif, T. Sandal, J. Legg, L. Thompson, et al., Increased tumor penetration of single-domain antibody-drug conjugates improves in vivo efficacy in prostate cancer models, Cancer Res. 80 (2020) 1268–1278.
[40] S.J. Walsh, J.D. Bargh, F.M. Dannheim, A.R. Hanby, H. Seki, A.J. Counsell, X. Ou, E. Fowler, N. Ashman, Y. Takada, et al., Site-selective modification strategies in antibody-drug conjugates, Chem. Soc. Rev. 50 (2021) 1305–1353.
[41] F. Lhospice, D. Brégeon, C. Belmant, P. Dennler, A. Chiotellis, E. Fischer, L. Gauthier, A. Boëdec, H. Rispaud, S. Savard-Chambard, et al., Site-Specific conjugation of monomethyl auristatin e to Anti-CD30 antibodies improves their pharmacokinetics and therapeutic index in rodent models, Mol. Pharm. 12 (2015) 1863–1871.

[42] J.A. Francisco, C.G. Cerveny, D.L. Meyer, B.J. Mixan, K. Klussman, D.F. Chace, S. X. Rejniak, K.A. Gordon, R. DeBlanc, B.E. Toki, et al., cAC10-vcMMAE, an anti-CD30-monomethyl auristatin E conjugate with potent and selective antitumor activity, Blood 102 (2003) 1458–1465.
[43] Y.V. Kovtun, C.A. Audette, M.F. Mayo, G.E. Jones, H. Doherty, E.K. Maloney, H. K. Erickson, X. Sun, S. Wilhelm, O. Ab, et al., Antibody-maytansinoid conjugates designed to bypass multidrug resistance, Cancer Res. 70 (2010) 2528–2537.
[44] K. von Schwarzenberg, T. Lajtos, L. Simon, R. Müller, G. Vereb, A.M. Vollmar, V-ATPase inhibition overcomes trastuzumab resistance in breast cancer, Mol. Oncol. 8 (2014) 9–19.
[45] M. Barok, H. Joensuu, J. Isola, Trastuzumab emtansine: mechanisms of action and drug resistance, Breast Cancer Res. 16 (2014) 1–12.
[46] H. Ding, M. Altai, W. Yin, S. Lindbo, H. Liu, J. Garousi, T. Xu, A. Orlova, V. Tolmachev, S. Hober, et al., HER2 - specific pseudomonas exotoxin A PE25 based fusions: influence of targeting domain on target binding, toxicity, and in vivo biodistribution, Pharmaceutics 12 (2020) 391.
[47] J. Garousi, H. Ding, E. von Witting, T. Xu, A. Vorobyeva, M. Oroujeni, A. Orlova, S. Hober, T. Gräslund, V. Tolmachev, Targeting her2 expressing tumors with a potent drug conjugate based on an albumin binding domain-derived affinity protein, Pharmaceutics (2021) 13.
[48] L. Yu, Y. Wang, Y. Yao, W. Li, Q. Lai, J. Li, Y. Zhou, T. Kang, Y. Xie, Y. Wu, et al., Eradication of growth of HER2-positive Ovarian cancer with trastuzumab-DM1, an antibody-cytotoxic drug conjugate in mouse xenograft model, Int. J. Gynecol. Cancer 24 (2014) 1158–1164.